Workshop on Astrophysical Opacities
ASP Conference Series, Vol. 515
C. Mendoza, S. Turck-Chièze, and J. Colgan, eds.

The IRON Project: Photoionization of Fe Ions

Sultana N. Nahar
Dept. of Astronomy, The Ohio State University, Columbus, OH 43210, USA;
nahar.1@osu.edu

Abstract. Initiated in 1991, the IRON Project has had two main objectives: (i) to study the characteristics of and calculate large-scale accurate datasets for atomic radiative and collisional processes; and (ii) to solve astrophysical problems based on reliable atomic data. It has given priority to the complex iron and iron-peak elements widely observed in the spectra of astrophysical plasmas. In the present report we illustrate the features of the dominant atomic process of photoionization that have been established under this project and the preceding Opacity Project and their importance in applications.

1. Introduction: Photoionization and the Opacity and Iron Projects

The photoionization of an ion of charge $+z$ can be direct

$$X^{+z} + h\nu \rightleftharpoons X^{+z+1} + \mathrm{e}^- \,, \tag{1}$$

giving a cross section with a smooth background, or in two steps when an intermediate doubly excited state is formed

$$X^{+z} + h\nu \rightleftharpoons (X^{+z})^{**} \rightleftharpoons X^{+z+1} + \mathrm{e}^- \,. \tag{2}$$

In a collisional framework, an electron colliding with the ion can form an intermediate state where two electrons are excited. It is called an *autoionizing state* if it lies above the ionization threshold since it decays either through autoionization (AI), when the outer electron is freely ejected in a radiationless process as the inner electron drops to the ground state, or via dielectronic recombination (DR) when the electron is captured by radiation damping emitting a photon

$$\mathrm{e}^- + X^{+z} \leftrightarrow (X^{+z-1})^{**} \leftrightarrow \left\{ \begin{array}{ll} \mathrm{e}^- + X^{+z} & \mathrm{AI} \\ X^{+z-1} + h\nu & \mathrm{DR} \end{array} \right\} \,. \tag{3}$$

In other words DR is the inverse of photoionization.

The autoionizing state is a quantum state of energy

$$E_x nl = E(X^{+z} \nu l)^{**} = E_x - \frac{z^2}{\nu^2} = E_x - \frac{z^2}{(n-\mu)^2} \,, \tag{4}$$

where E_x is an excited state of the residual or core ion relative to its ground state and nl is the quantum level of the outer electron. $\nu = n - \mu$ is basically the effective quantum

number and μ the quantum defect describing the departure from a pure hydrogenic state. An autoionizing state gives rise to a resonance in the photoionization cross section $\sigma_{\rm PI}$. Levels $E_x nl$ below an excited threshold E_x form a Rydberg series of either bound states or quasi-bound resonances, the latter showing similar features but can be difficult to identify when lying close together. The resonance strength varies depending on the values of the excitation rate coefficients and interference. The strong Seaton resonances (Yan & Seaton 1987), in particular, occur when the core ion absorbs the photon (to be discussed in Section 3.4).

The autoionization rate A_a is normally about $10^{15}-10^{16}$ s^{-1} and remains about the same for all the effective quantum numbers ν of the Rydberg resonance series. The radiative decay rate A_r is about $10^{8}-10^{12}$ s^{-1} for low-lying levels, but increases as ν^3 becoming comparable to A_a near and below the excited threshold of the residual ion. Both rates can be comparable at lower ν for the highly charged He- and Li-like ions. In such cases the radiation damping of autoionizing resonances can be treated using a scheme based on fits of the dipole matrix of the autoionizing resonance (Sakimoto et al. 1990; Pradhan & Zhang 1997; Zhang et al. 1999).

The Opacity Project (OP, Seaton 1987; The Opacity Project Team 1995, 1997) carried out the first systematic study of photoionization of the ground and excited states for astrophysically important atoms and ions from H to Fe. The atomic and opacity data computed are available in the databases TOPbase[1] and OPserver[2] (Mendoza et al. 2007), respectively. The follow-up of the OP, namely the IRON Project (IP, Hummer et al. 1993), included relativistic fine-structure effects to study the collisional and radiative processes of key ionic species and of iron and iron-peak elements. A significant amount of calculated data obtained in the IP are available online from TIPbase[3] and NORAD-Atomic-Data (NORAD[4]).

This report presents a review of the features in the photoionization of Fe ions elucidated in the OP and IP that are relevant in the study of the solar opacity.

2. Theory

To study photoionization the *R*-Matrix method relies on the close-coupling (CC) approximation for the wave-function expansion (e.g., Berrington et al. 1987; Pradhan & Nahar 2011). The CC approximation is the most precise theoretical approach to compute resonances formally. Under the OP and IP the *R*-Matrix method (e.g., Burke & Robb 1975) and its suite of codes were developed extensively (Seaton 1987; Hummer et al. 1993; Berrington et al. 1987, 1995; Pradhan & Nahar 2011). Furthermore, relativistic fine-structure effects have been included via the Breit–Pauli Hamiltonian in a version referred to as BPRM. A brief outline of the *R*-Matrix numerical method and packages is given in this volume by Pradhan & Nahar (2018).

---

[1] `http://cdsweb.u-strasbg.fr/topbase/topbase.html`

[2] `http://opacities.osc.edu`

[3] `http://cdsweb.u-strasbg.fr/tipbase/home.html`

[4] `http://norad.astronomy.ohio-state.edu`

3. Results and Discussions

The central-field and distorted-wave approximations can give approximate photoionization background cross sections $\sigma_{\rm PI}$ (e.g., Reilman & Manson 1979; Gu 2008). Rates for bound–free transitions calculated with an atomic structure method (e.g., Eissner et al. 1974) can be broadened with a profile function to represent resonances in $\sigma_{\rm PI}$ (e.g., Simon et al. 2010), but they do not characterize accurately their properties and can introduce large uncertainty. In Sections 3.1–3.8 we illustrate the resonance features obtained in *R*-Matrix calculations.

3.1. Resonances in a Two-Electron System

A hydrogenic ion has no core electron and, hence, cannot form a doubly excited autoionizing state, i.e., a resonance. The $\sigma_{\rm PI}$ of the 2p ^{2}P$^{\rm o}$ state of the H-like iron ion Fe XXVI in Fig. 1 (left panel) shows a monotonic smooth decay with photon energy (Nahar et al. 2001). On the other hand, the $\sigma_{\rm PI}$ for the 1s2p ^{1}P$^{\rm o}$ state of He-like Fe XXV (Fig. 1 right panel) decays to a hydrogenic ion at the lower energies, but exhibits strong high peak resonances of the type $2l3l'$, $2l4l'$, etc. converging to the $n = 2$ states of the core ion (Nahar et al. 2001). A considerable step-like enhancement is seen at the excited $n = 2$ threshold energy of ~ 670 Ry (indicated with an arrow) due to the dipole-allowed 1s–2p transition in the core ion. These features have been generated with BPRM using a 10-CC (10-level) wave-function expansion of the core ion that can be excited up to the 4f level. These structures were not found in the earlier OP work where single-core-state calculations were performed (data in TOPbase by M. J. Seaton, unpublished).

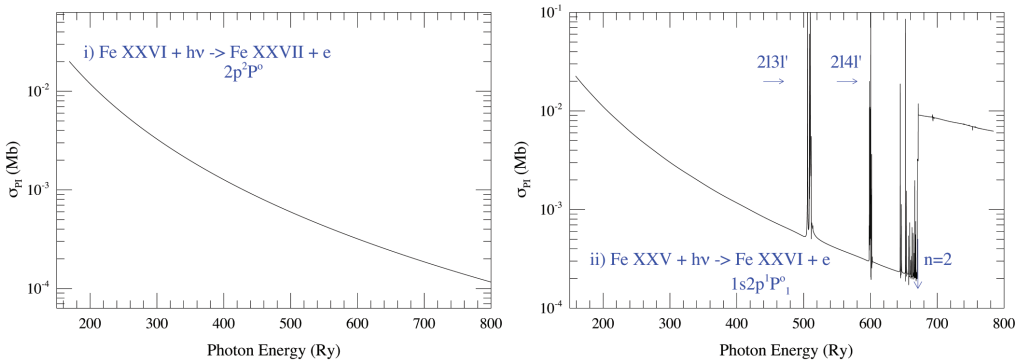

Figure 1. Photoionization cross sections $\sigma_{\rm PI}$ illustrating the smooth decay of the 2p ^{2}P$^{\rm o}$ state of H-like Fe XXVI (*left panel*) and the resonant features in the 1s2p ^{1}P$^{\rm o}$ state of He-like Fe XXV (Nahar et al. 2001, *right panel)*. The high peak resonances of type $2l3l'$, $2l4l'$, etc. and the sharp step at the $n = 2$ threshold (~ 670 Ry) are due to the 1s–2p dipole-allowed transition in the core ion.

3.2. Resonances in Ions with a Large Number of Electrons

A larger number of electrons in the core ion usually increases the number of excitations in the lower energy region and, hence, the number of Rydberg series of autoionizing resonances near the ionization threshold. These resonances are important in the description of low to medium high-temperature plasmas in numerical integrals containing an exponential factor such as recombination rates. Seaton resonances (see

Section 3.4) are usually more prominent at higher energy and thus have more impact on high-temperature plasmas.

Fig. 2 (left panel) shows the $\sigma_{\rm PI}$ for the $3d^6 4s\ ^6D$ ground state of Fe II obtained from the largest atomic calculations at the time (Nahar & Pradhan 1994). The wave-function expansion included 83 states from the $n = 2$–3 complexes of the Fe III core ion. This ion shows strong electron–electron correlation effects by generating extensive resonances near the ionization threshold and over the energy range of about 1.3 Ry spanned by the 83 states. The earlier $\sigma_{\rm PI}$ obtained under the OP (Sawey & Berrington 1992) had incomplete correlation interactions and, thus, produced only the general background, which is much lower than present values.

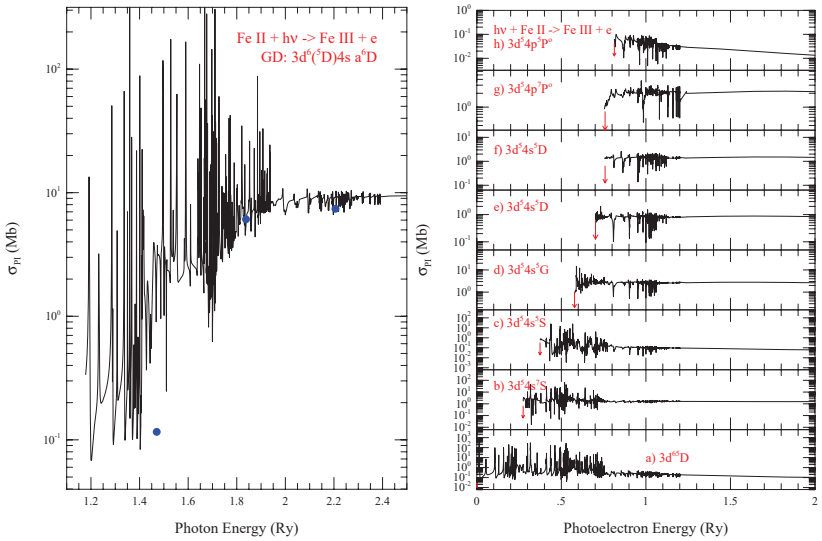

Figure 2. *Left*: $\sigma_{\rm PI}$ of the $3d^6 4s\ ^6D$ ground state of Fe II showing extensive resonances in the low-energy region due to strong electron–electron interaction among 25 electrons (Nahar & Pradhan 1994). The blue dots are from the central-field approximation of Reilman & Manson (1979). *Right*: Partial $\sigma_{\rm PI}$ of the ground state $3p^6 4s\ ^6D$ leaving the core ion in the ground (a) and 7 other excited states (b–h, thresholds denoted by arrows) as specified in the panels.

The total $\sigma_{\rm PI}$, such as that of Fe II in this figure, is obtained by summing up the partial $\sigma_{\rm PI}$ corresponding to ionization leaving the residual ion in the ground and various excited states. With the increase of photon energy, the ion is ionized to higher excitations of the core ion. The right panel of Fig. 2 presents the partial $\sigma_{\rm PI}$ with resonant structures leaving the residual ion in the ground state (a) and seven (b–h) excited states (Nahar & Pradhan 1994). The partial cross sections help resonance identification.

3.3. Photoionization of Excited Equivalent Electron States

The ground-state photoionization cross section typically has less features than those of excited states (Fe II in Fig. 2 is an exception) and a slow background decay. Other states showing slow background decays in $\sigma_{\rm PI}$ are equivalent electron states; however, they have more resonant features in the lower energy region. These states are important contributors to processes such as electron–ion recombination. Fig. 3 depicts the $\sigma_{\rm PI}$ of two equivalent electron states of Fe IV obtained using a 16-CC wave-function expansion

(Nahar & Pradhan 2005) that shows the typical features of such states. Narrow Rydberg resonances belonging to various low-lying excited core states arise prominently at and near the ionization threshold, and a large background remains beyond the highest excitation threshold of the core ion included in the wave-function expansion. Equivalent electron states do not show the wide Seaton resonances described in Section 3.4.

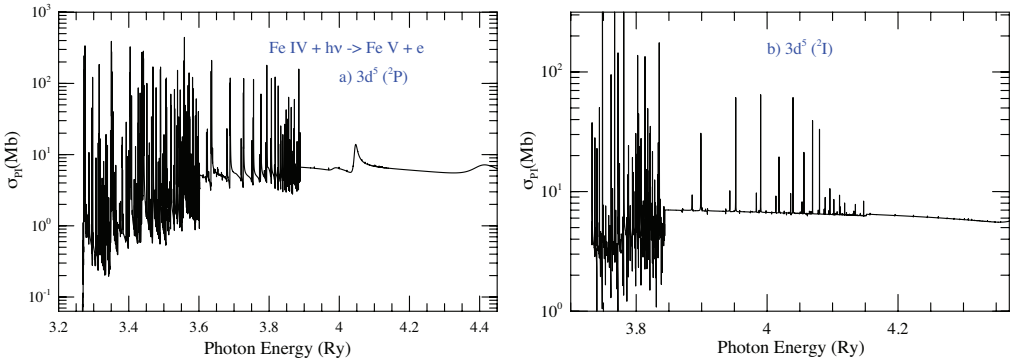

Figure 3. $\sigma_{\rm PI}$ for the two equivalent states $3d^5\ ^2P$ and $3d^5\ ^2D$ of Fe IV illustrating the predominant background dominance at higher energies.

3.4. Seaton Resonances Due to PEC

A Seaton resonance is different from a Rydberg resonance. It arises in the $\sigma_{\rm PI}$ of an excited state i when the core-ion ground state absorbs the photon: a photoexcitation of the core (PEC) to a dipole-allowed state of transition energy E_x. The outer electrons remain inactive temporarily as "spectators" during the transition, but lead to ionization as the excited core ion decays back to the ground state. The PEC resonance interferes with the Rydberg resonances manifesting itself as a wider peak with a background often enhanced by orders of magnitude at an energy $E_x - E_i$ from the ionization threshold energy E_i of the ith state. Fig. 4 illustrates the characteristics of a Seaton resonance (indicated with arrows) in the $\sigma_{\rm PI}$ of the $3d^5(^6S)7p\ ^5P^o$ excited state and of a number of other excited states of Fe III (Nahar 1996). The Seaton resonance is more distinct in the higher excited states (right panel of Fig. 4b–f). Interference from electron–electron correlations of low-lying excited states can reduce the prominence of the structure and may appear slightly shifted (right panel of Fig. 4a–b). Seaton resonances cause the high-energy behavior of $\sigma_{\rm PI}$ to be non-hydrogenic for low to fairly high lying excited states, contradicting their assumed hydrogenic $1/\nu^3$ behavior with energy.

3.5. Resonances near the Ionization Threshold Due to Relativistic Channels

Relativistic effects are important when electrons are moving very fast due to a high nuclear charge of a heavy high-Z element and/or a highly charged ion such as Fe XXV. Relativistic effects split the resonances into their fine-structure components causing a large number of narrower features. However, we have found that the fine-structure effects can introduce strong resonances at and near the ionization threshold region of $\sigma_{\rm PI}$ for low to medium-high Z elements (e.g., for P II by Nahar et al. 2017), but not significantly for the rest of the energy region. Fig. 5 presents the $\sigma_{\rm PI}$ of the $2s2p^3\ ^5S^o$ state in carbon-like Fe XXI, demonstrating the relativistic fine-structure effect of introducing

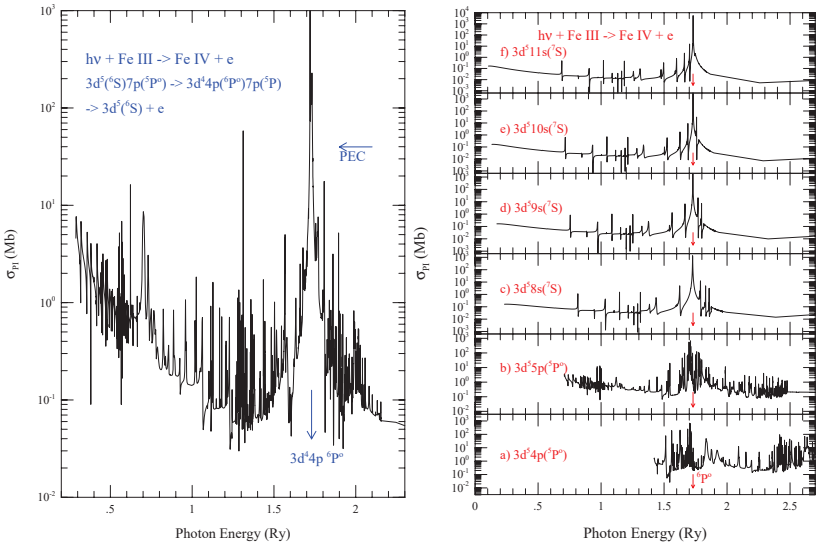

Figure 4. *Left*: $\sigma_{\rm PI}$ of the $3d^5(^6S)7p\ ^5P^o$ excited state of Fe III exhibiting a huge Seaton resonance at 1.73 Ry, namely, the transition energy for a PEC from the $3d^5\ ^6S$ ground state to the excited state $3d^44p\ ^6P^o$ of the Fe IV core ion. *Right*: σ_{PI} of two series of excited states of Fe III: (a) $3d^54p\ ^5P^o$; (b) $3d^55p\ ^5P^o$; (c) $3d^58s\ ^7S$; (d) $3d^59s\ ^7S$; (e) $3d^510s\ ^7S$; and (f) $3d^511s\ ^7S$ illustrating that, regardless of the state, the energy position (indicated with the arrows) of the Seaton resonance remains the same (Nahar 1996).

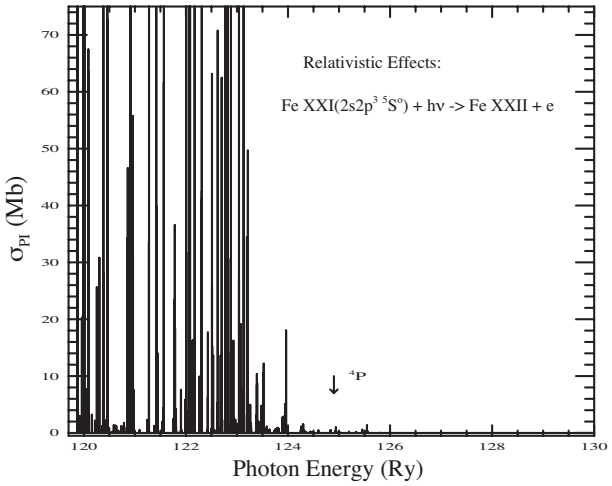

Figure 5. Cross section $\sigma_{\rm PI}$ of the excited $2s2p^3\ ^5S^o$ state of Fe XXI showing narrow, high peak resonances below the first excited core ion threshold $2s2p^2\ ^4P$ (pointed by arrow) formed by fine-structure couplings (Nahar 2008b).

strong resonances near threshold not allowed in the *LS* coupling approximation (Nahar 2008a). In *LS* coupling the state $2s2p^3\ ^5S^o$ photoionizes only to $2s2p^2(^4P)\,\epsilon d\ ^5P$ or $2s2p^2(^4P)\,\epsilon s\ ^5P$ leaving the core ion in the $2s2p^2\ ^4P$ state. This means that $\sigma_{\rm PI}$ is zero below the ^4P state (indicated by an arrow in Fig. 5). However, in reality resonances

can form below the ^{4}P threshold by fine-structure coupling effects. The fine-structure channels with the excited core ion $2s2p^2(^4P)\,nd, ns\ ^5P_{1,2,3}$ are allowed to couple with those of the ground levels $2s^22p(^2P^o{}_{1/2,3/2})\,\epsilon p\ ^{1,3}P_{1,2,3}$. This leads to radiationless autoionization below the ^{4}P threshold and the introduction of the narrow and high peak resonances with an almost negligible background cross section (Nahar 2008a). These resonances are found to make significant contributions in low-temperature plasmas.

3.6. Resonant Enhancement Due to $\Delta n = 1$

The wave-function expansions considered by the OP included core-ion states from the n complex of the outer electron, i.e., $\Delta n = 0$. It was assumed that the high lying states (i) are not common in the astrophysical plasmas of interest and (ii) have weak couplings with the lower ones causing weaker resonances; however, the step increase in the decaying $\sigma_{\rm PI}$ at the inner-shell ionization threshold of the core ion was included. Later studies (e.g., for oxygen ions by Nahar 1998) have found that resonances due to high lying core-ion states with $\Delta n = 1$ are much stronger than those with $\Delta n = 0$. Thus, if neglected the integrated cross section may be underestimated.

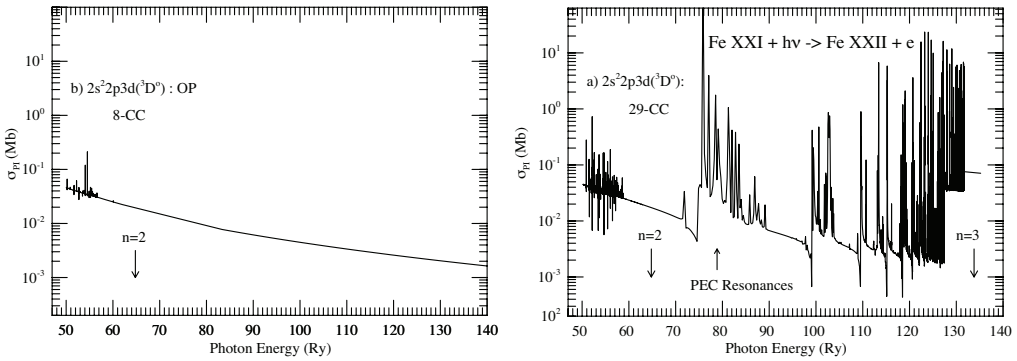

Figure 6. Effect of core-ion excitations on $\sigma_{\rm PI}$ of the $2s^22p3d\ ^3D^o$ state of Fe XXI to $\Delta n = 0$ states (*left panel*, 8-CC, Luo & Pradhan 1989) and to $\Delta n = 1$ states (*right panel*, 29-CC, Nahar 2008a). Comparison shows: (i) the wide Seaton resonances in the energy range of 73–82.5 Ry; (ii) high peak resonances by stronger correlation effects; and (iii) enhanced background at higher energy by excitations to $n = 3$ states.

Fig. 6 shows the $\sigma_{\rm PI}$ of the $2s^22p3d\ ^3D^o$ excited state of Fe XXI obtained using (a) a 29-CC wave-function expansion that includes $\Delta n = 0, 1$ states (Nahar 2008a) and (b) an 8-CC expansion that only accounts for $\Delta n = 0$ states (Luo & Pradhan 1989). The first complex of narrow Rydberg resonances (identified with an arrow at $n = 2$) belongs to excitations of the core ion to $\Delta n = 0$ states; that is, to states with $n = 2$. They are less prominent than those arising from $n = 3$ states in the higher energy region, where the features are more extensive and stronger and span a larger energy range. The latter can be divided into two groups: the broader Seaton resonances in the photon energy range 73–82 Ry with 8 possible PECs; and a series of narrow Rydberg resonances belonging to various states of the $n = 3$ complex in the rest of the high-energy region. The high-energy background is also considerably enhanced. Such strong effects were not unexpected in Fe XXI due to the large energy gap ($\sim$ 50 Ry) between the $n = 2$ and $n = 3$ states, their prominence caused by the larger radiative decay rates of the latter.

3.7. Convergence of the Enhancement Due to Resonances

The photoionization of Fe XVII has been studied to determine the impact of the $\Delta n = 2$ excitations of the core ion. The $\sigma_{\rm PI}$ of this ion contributes significantly to the plasma opacity near the boundary of the radiative and convection zones of the Sun. The $\sigma_{\rm PI}$ determined with a wave function composed of 60 fine-structure target levels (30 *LS* states) with $\Delta n = 0, 1$ (Nahar et al. 2011a) showed considerable amount of photoabsorption (see the $\sigma_{\rm PI}$ for the $2s^2 2p^5 3d\ ^1D^o$ state of Fe XVII in Fig. 7, black curve) not seen in that computed with a 2-CC target expansion (TOPbase, blue curve in Fig. 7). The enhancements in $\sigma_{\rm PI}$ from the 60-CC calculation increases the Rosseland mean opacity for Fe XVII by 20% relative to 2-CC, and could be a possible source for the discrepancy with measured values (Bailey et al. 2015).

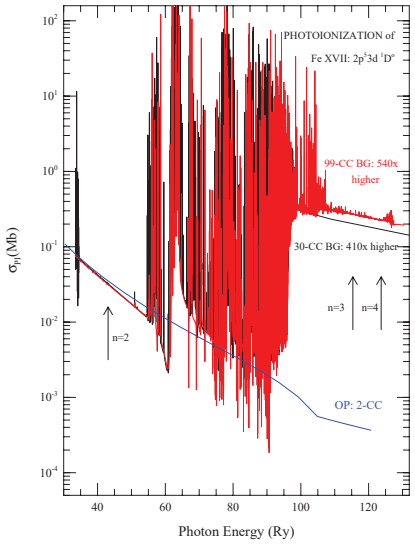

Figure 7. Comparison of the $\sigma_{\rm PI}$ for the $2s^2 2p^5 3d\ ^1D^o$ excited state of Fe XVII from three calculations: (i) blue curve, 2-CC; (ii) black curve, 30-CC (60 fine-structure levels) by Nahar et al. (2011a); and (iii) red curve, 99–CC by Nahar & Pradhan (2016). The strong peak resonances and huge background enhancement by orders of magnitude are due to $\Delta n = 1$ states. The weaker resonances of $n = 4$ excitations indicate the convergence of resonant contributions with higher n. Arrows indicate the energy limits for the $n = 2$–4 states of the core ion.

The most recent study of $\sigma_{\rm PI}$ for Fe XVII (Nahar & Pradhan 2016) used a larger wave-function expansion of 99 states that included the $n = 4$ states ($\Delta n = 0, 1, 2$) (red curve in Fig. 7). Arrows indicate the energy positions for the highest $n = 2, 3, 4$ states. We neither note a significant enhancement from $n = 4$ excitations, resonances being much weaker, nor a negligible enhancement in the background cross section (red curve) as compared to those from $n = 3$ states (black curve). This demonstrates that convergence of the resonant contribution from core excitations to higher n states has been reached. The narrow resonances close to the ionization threshold in the black curve of 30-CC are from fine-structure couplings of the relativistic BPRM method. Convergence with $\Delta n = 2$ excitations in the core ion was also found in Fe XXV (Nahar et al. 2001).

3.8. Resonances below K-Shell Ionization

Resonances below the K-shell threshold may show multiple ionization effects. Typically resonances become weaker and the background decreases with higher photon energy. However, resonances below the K shell tend to rise again due to the higher 1s–2p excitation rates. Their peaks can be orders of magnitude higher than the K edge level: over 2 orders of magnitude for Fe and over 3.5 orders for Au as shown in Fig. 8 (Pradhan et al. 2009; Lim et al. 2013), where these resonances are superimposed on the background cross sections of the atoms available at the NIST[5] website. The resonance complex in Fig. 8 corresponds to allowed Kα (1s–2p) transitions of all ionization stages from Ne- to He-like ions following K-shell ionization. In the Auger process, where an L-shell electron drops down to fill the K-shell vacancy, a Kα photon is emitted. This photon can knock out an L-shell electron creating an additional hole. Continuation of this process to higher levels can lead to Coster–Kronig cascading; that is, multiple ionization stages as photons and electrons are emitted. However, such a cascade can occur if the photon energy matches those of the resonances presented in Fig. 8 (Pradhan et al. 2009). The enhanced resonant photoionization can result in resonant Kα fluorescence below the K-shell ionization of each ionization stage of Ne- to He-like ions, and was observed by Vinko et al. (2012) and interpreted by Nahar & Pradhan (2015).

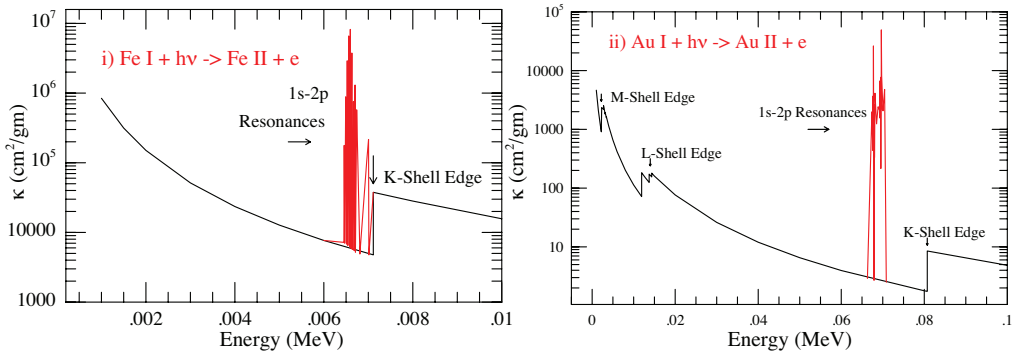

Figure 8. High peak resonances below the K-shell ionization threshold of (i) iron (*left panel*) and (ii) gold arising from Kα 1s–2p transitions (*right panel*). The resonances correspond to all the allowed Kα transitions of the Ne- to He-like ions as the element goes through multiple ionization stages at a resonant energy (Pradhan et al. 2009).

4. Accuracy and Completeness

Both accuracy and completeness are needed in calculations of photoionization cross sections in benchmarks with high-precision experiments and in the solution of astrophysical problems. Accuracy depends on the number of states included in the wavefunction expansion, on the number of configurations included for accurate representation of correlation effect, and on the number of grid points to resolve the resonances. Completeness implies cross sections for a large number of bound states. These have

[5] `http://physics.nist.gov/PhysRefData/Xcom/html/xcom1.html`

been the objectives of both the OP and IP. An example of accuracy is given in Fig. 9 depicting the $\sigma_{\rm PI}$ of the complex ion P II, where the combined resonant features observed in the sophisticated setup of the Advanced Light Source at Berkeley National Lab. (panel a) are being identified with *R*-Matrix calculations in panels b–f (Nahar et al. 2017). The comparison shows that the observed features belonging to the ground and low-lying metastable levels are reproduced by theory.

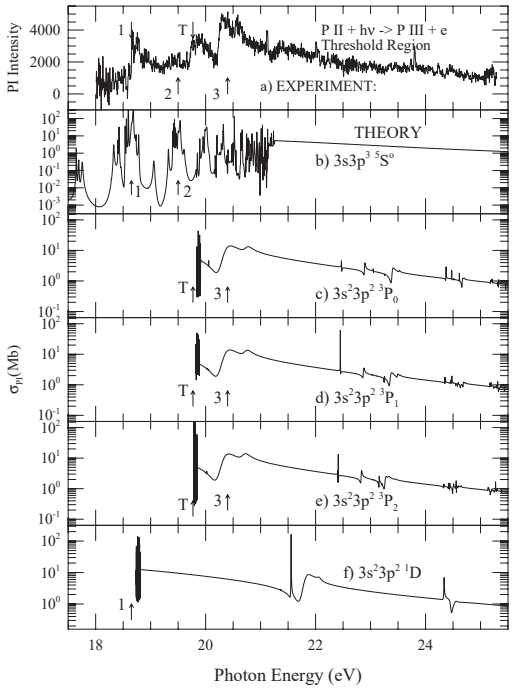

Figure 9. Benchmarks of the $\sigma_{\rm PI}$ of P II: (a) combined features observed in experiment; (b)–(f) theoretical identification of observed features (1, 2, 3, T) generated by the excited level 3s3p^3 ^{5}S$^o_2$ (b), ground level 3s^{2}3p^2 ^{3}P$_0$ (c), and the three excited levels 3s^{2}3p^2 ^{3}P$_{1,2}$ and 3s^{2}3p^2 ^{1}D$_2$ (d)–(f). Agreement is seen in the reproduced observed features (Nahar et al. 2017). [Reprinted from Fig. 3 of Nahar et al. (2017), Copyright (2017), with permission from Elsevier.]

5. Conclusion

The extensive study of atomic photoionization carried out under the Iron and Opacity Projects has established a number of characteristic features of this process. They have a critical impact on astrophysical applications such as the determination of plasma opacity, elemental abundances, and ionization fractions. A detailed and accurate study of this process and the computation of large-scale atomic datasets for completeness are required in the precise analysis of astrophysical spectra.

Acknowledgments. Partial support by DOE grant DE-FG52-09NA29580 and NSF grant AST-1312441 are acknowledged. Computations were carried out at the Ohio Supercomputer Center, Columbus.

References

Bailey, J. E., Nagayama, T., Loisel, G. P., et al. 2015, Nature 517, 56
Berrington, K. A., Burke, P. G., Butler, K., et al. 1987, J. Phys. B – At. Mol. Opt., 20, 6379
Berrington, K. A., Eissner, W., & Norrington, P. H., 1995, Comput. Phys. Commun., 92, 290
Burke, P. G., & Robb, W. D. 1975, Adv. At. Mol. Phys., 11, 143
Eissner, W., Jones, M., & Nussbaumer, H. 1974, Comput. Phys. Commun. 8, 270
Gu, M. F. 2008, Can. J. Phys., 86, 675
Hummer, D. G., Berrington, K. A., Eissner, W., et al. 1993, A&A, 279, 298
Lim, S., Montenegro, M., Pradhan A. K., et al. 2013, in World Congress on Medical Physics and Biomedical Engineering May 26-31, 2012, Beijing, China, edited by M. Long (Berlin-Heidelberg, Germany: Springer), vol. 39 of IFMBE Proceedings, 2248
Luo, D., & Pradhan, A. K. 1989, J. Phys. B – At. Mol. Opt., 22, 3377
Mendoza, C., Seaton, M. J., Buerger, P., et al. 2007, MNRAS, 378, 1031
Nahar, S. N. 1996, Phys. Rev. A, 53, 1545
— 1998, Phys. Rev. A, 58, 3766
— 2008a, J. Quant. Spectrosc. Ra., 109, 2417
— 2008b, J. Quant. Spectrosc. Ra., 109, 2731
Nahar, S. N., Eissner, W., Chen, G. X., & Pradhan, A. K. 2003, A&A, 408, 789
Nahar, S. N., Hernández, E. M., Hernández, L., et al. 2017, J. Quant. Spectrosc. Ra., 187, 215
Nahar, S. N., Montenegro, M., Eissner, W., & Pradhan, A. K. 2010, Phys. Rev. A. 82, 065401
Nahar, S. N., & Pradhan, A. K. 1994, J. Phys. B – At. Mol. Opt., 27, 429
— 2005, A&A, 437, 345
— 2015, J. Quant. Spectrosc. Ra., 155, 32
— 2016, Phys. Rev. Lett., 116, 235003
Nahar, S. N., Pradhan, A. K., Chen, G. X., & Eissner, W. 2011a, Phys. Rev. A, 83, 053417
Nahar, S. N., Pradhan, A. K., & Montenegro, K. 2011b, in Simulations in Nanobiotechnology, edited by K. Eom (Boca Raton, FL: CRC Press), chap. 9, 305
Nahar, S. N., Pradhan, A. K., & Zhang, H. L. 2001, ApJS, 133, 255
Pradhan, A. K., & Nahar, S. N. 2011, Atomic Astrophysics and Spectroscopy (Cambridge, UK: Cambridge University Press)
— 2018, this volume
Pradhan A. K., Nahar, S. N., Montenegro, N., et al. 2009, J. Phys. Chem. A, 113, 12356
Pradhan, A. K. & Zhang, H. L. 1997, J. Phys. B – At. Mol. Opt., 30, L571
Reilman, R. F., & Manson, S. T. 1979, ApJS, 40, 815
Sakimoto, K., Terao, M., & Berrington, K. A. 1990, Phys. Rev. A, 42, 291
Sawey, P. M. J., & Berrington, K. A. 1992, J. Phys. B – At. Mol. Opt., 25, 1451
Seaton, M. J. 1987, J. Phys. B – At. Mol. Opt., 20, 6363
Simon, M. C., Schwarz, M., Epp, S. W., et al. 2010, J. Phys. B – At. Mol. Opt., 43, 065003
The Opacity Project Team. 1995, The Opacity Project (Bristol, UK: IOP Publishing), vol. 1
— 1997, The Opacity Project (Bristol, UK: IOP Publishing), vol. 2
Vinko, S. M., Ciricosta, O., Cho, B. I., et al. 2012, Nature 482, 59
Yan, Y. & Seaton, M. J. 1987, J. Phys. B – At. Mol. Opt., 20, 6409
Zhang, H. L., Nahar, S. N., & Pradhan, A. K. 1999, J. Phys. B – At. Mol. Opt., 32, 1459